Helical Topological Superconducting Pairing at Finite Excitation Energies

Masoud Bahari,[1,2,*] Song-Bo Zhang,[3,4] Chang-An Li,[1,2] Sang-Jun Choi,[5] Philipp Rüßmann,[1,6] Carsten Timm,[2,7] and Björn Trauzettel[1,2]

[1]Institute for Theoretical Physics and Astrophysics, University of Würzburg, D-97074 Würzburg, Germany
[2]Würzburg-Dresden Cluster of Excellence ct.qmat, Germany
[3]Hefei National Laboratory, Hefei, Anhui, 230088, China
[4]International Center for Quantum Design of Functional Materials (ICQD), University of Science and Technology of China, Hefei, Anhui, 230026, China
[5]Department of Physics Education, Kongju National University, Gongju 32588, Republic of Korea
[6]Peter Grünberg Institut, Forschungszentrum Jülich and JARA, D-52425 Jülich, Germany
[7]Institute of Theoretical Physics, Technische Universität Dresden, 01062 Dresden, Germany

(Received 21 October 2022; revised 19 April 2024; accepted 15 May 2024; published 24 June 2024)

We propose helical topological superconductivity away from the Fermi surface in three-dimensional time-reversal-symmetric odd-parity multiband superconductors. In these systems, pairing between electrons originating from different bands is responsible for the corresponding topological phase transition. Consequently, a pair of helical topological Dirac surface states emerges at finite excitation energies. These helical Dirac surface states are tunable in energy by chemical potential and strength of band splitting. They are protected by time-reversal symmetry combined with crystalline twofold rotation symmetry. We suggest concrete materials in which this phenomenon could be observed.

DOI: 10.1103/PhysRevLett.132.266201

Introduction.—The search for intrinsic topological superconductors has been an active research area in the condensed matter community for many years [1–5]. In weakly interacting systems, the essential ingredient for intrinsic topological phase transitions (TPTs) is a weak attractive electron-electron interaction appearing close to the Fermi surface. This results in particular bulk properties including topological superconducting gaps [6–18], possibly with nodes [19–28]. Because of particle-hole symmetry, the bulk-boundary correspondence allows for emergent Majorana boundary states protected by band topology.

Finite energy (FE) Cooper pairing is a particular type of pairing that can happen away from the Fermi surface [29–37]. It arises from multiband effects in superconductors [38–55]. Dips in the density of states at FEs is a particular spectral feature of such pairing found in hybrid structures based on the superconducting proximity effect of $NbSe_2$ in the topological insulators $BiSbTe_{1.25}Se_{1.75}$ [56] and Bi_2Se_3 [57]. In this Letter, we show that TPTs can be exclusively induced by FE Cooper pairing emerging from time-reversal-symmetric odd-parity multiband superconductors. The interplay of spin-orbit coupling and electron-phonon interaction allows for the formation of unconventional FE Cooper pairing with topologically nontrivial order. Bulk band crossings are partially gapped out in momentum space at FEs due to odd-parity superconductivity. This leads to TPTs as evidenced by helical topological Dirac surface states at finite excitation energies. Such surface states are composed of electrons and holes with different magnetic quantum numbers. They are distinct from conventional Majorana boundary states due to broken particle-hole symmetry away from the Fermi energy. The helical Dirac points are (i) protected topologically by time-reversal $\hat{T}$ symmetry combined with crystalline twofold rotation as we specify below, and (ii) tunable in energy by chemical potential and strength of band splitting.

To observe FE Cooper pairing, the normal state should have at least two energy bands with the same sign of curvature close to the Fermi energy. The bands need to have different effective masses. Therefore, our results are relevant for a broad range of multiband superconductors as we elaborate on here.

To capture the underlying physics, we develop a theory for generic superconducting multiband systems with four-valued local degrees of freedom. For concreteness, we work with a model Hamiltonian describing the band structure of electrons with effective angular momentum $j = 3/2$ near the Fermi energy. However, the formalism is not restricted to this particular choice of angular momentum quantum numbers.

Model.—We start with the Luttinger-Kohn Hamiltonian $\hat{\mathcal{H}}_{\mathbf{k}} = \alpha|\mathbf{k}|^2 + \beta(\mathbf{k}\cdot\mathbf{J})^2 - \mu$, which describes $j = 3/2$ electrons within the Γ_8 bands [24,58–60]. The kinetic, symmetric spin-orbit-coupling, and chemical potential terms are parameterized by α, β, and μ, respectively. $\mathbf{k} = (k_x, k_y, k_z)$ is the three-dimensional (3D) momentum and $\mathbf{J} = (\hat{J}_x, \hat{J}_y, \hat{J}_z)$ are the 4×4 spin matrices in the $j = 3/2$

formalism. The normal state has a pair of doubly degenerate quadratic energy bands given by $E^{+}_{\mathbf{k}} = (\alpha + 9\beta/4)|\mathbf{k}|^2 - \mu$ and $E^{-}_{\mathbf{k}} = (\alpha + \beta/4)|\mathbf{k}|^2 - \mu$. The chemical potential μ should fulfill $|\mu| < N\hbar\omega_D$, where ω_D is the Debye frequency and $N = 1.25 + \alpha/\beta$ is a material dependent number. While $\hat{\mathcal{H}}_{\mathbf{k}}$ preserves O(3) symmetry, our predictions are generic and can be applied to systems with relevant point group symmetry in the normal state [61].

The superconducting properties of the system can be captured by the Bogoliubov–de Gennes (BdG) Hamiltonian

$$\hat{H}(\mathbf{k}) = \begin{pmatrix} \hat{\mathcal{H}}_{\mathbf{k}} & \hat{\Delta}_{\mathbf{k}} \\ \hat{\Delta}^{\dagger}_{\mathbf{k}} & -\hat{\mathcal{H}}^{T}_{-\mathbf{k}} \end{pmatrix}, \tag{1}$$

where $\hat{\mathcal{H}}_{\mathbf{k}}$ is the inversion-symmetric normal part and $\hat{\Delta}_{\mathbf{k}}$ is a 4×4 pairing matrix describing pairing of electrons with four-valued degrees of freedom. Generally, the explicit form of $\hat{\Delta}_{\mathbf{k}}$ depends on the basis of the system. For concreteness, we focus on systems with cubic point group O_h. In this case, $\hat{\Delta}_{\mathbf{k}}$ can be expanded into irreducible tensor operators of irreducible representations (irreps) of O_h [34,63–65].

Topology at finite energies.—The prerequisite for TPTs away from the Fermi energy is that the $E^{+}_{\mathbf{k}}$ electron and $-E^{-}_{\mathbf{k}}$ hole bands cross each other. These band crossings become anti-crossings in the presence of odd-parity FE Cooper pairing as we explain in detail in the Supplemental Material [62]. For concreteness, we consider the A_{2u} (p-wave septet) pairing given by $\hat{\Delta}_{\mathbf{k}} = \Delta(\mathbf{k}\cdot\hat{\mathbf{T}})\hat{\mathcal{R}}$, where Δ is the pairing strength, $\hat{\mathcal{R}} = e^{i\pi\hat{J}_y}$ is the fermionic antisymmetry factor, and $\hat{T}_i = \{\hat{J}_i, \hat{J}^2_{i+1} - \hat{J}^2_{i+2}\}$ with $i+1 = y$ if $i = x$, etc., cyclically [60,63]. Note that p-wave septet pairing has been argued to be the favorable pairing symmetry in systems with cubic symmetry [60,66,79]. Although we focus on this specific pairing channel, our qualitative results are general. They apply to several odd-parity pairing channels summarized in Table. I.

TABLE I. TPTs at FEs in p-wave pairing channels distinguished by cubic irreps (first column) and their components (second column). The direction of TPTs is denoted in the third column. The last column indicates the FE pairing potential responsible for TPTs. The pairing matrices for the given irreps are given in the Supplemental Material [62,80].

O_h		$\mathbf{k}$	$\hat{\Delta}^{+-}_{\mathbf{k}} = \Delta\times$
E_u	$E_u^{(2)}$	$(0,0,k_z)$	$k_z\hat{\tau}_0$
T_{2u}	$T_{2u}^{(1)}$	$(0,0,k_z)$	$k_z\hat{\tau}_z$
	$T_{2u}^{(2)}$	$(0,k_y,0)$	$k_y\hat{\tau}_x$
	$T_{2u}^{(3)}$	$(k_x,0,0)$	$ik_x\hat{\tau}_x$
A_{2u}		$(k_x,0,0)$	$-k_x\hat{\tau}_0$
		$(0,k_y,0)$	$-ik_y\hat{\tau}_z$
		$(0,0,k_z)$	$k_z\hat{\tau}_0$
T_{2u}	$T_{2u}^{(1)}$	$(0,0,k_z)$	$k_z\hat{\tau}_z$
		$(\pm k,\pm k,0)$	$k(\pm\hat{\tau}_0 \pm i\hat{\tau}_z)$
	$T_{2u}^{(2)}$	$(k_x,0,0)$	$k_x\hat{\tau}_x$
		$(0,\pm k,\pm k)$	$k(\hat{\tau}_y \pm \hat{\tau}_z/3)$
	$T_{2u}^{(3)}$	$(0,k_y,0)$	$k_y\hat{\tau}_x$
		$(\pm k,0,\pm k)$	$k(\pm\hat{\tau}_0/3 - i\hat{\tau}_y)$

Without loss of generality, we illustrate our predictions for the [001] direction (i.e., $k_x = k_y = 0$). We observe in Fig. 1(a) that the bulk bands, i.e., electron $E^{+}_{k_z}$ and hole $-E^{-}_{k_z}$ branches, do not touch each other for $\mu = -5.7\Delta$ close to $k_z = \pi$ away from the Fermi surface. In this case, the system exhibits a topologically trivial phase. Increasing slightly the Fermi energy to $\mu = -5.5\Delta$, this makes the two bands touch each other. For $\mu = -5.2\Delta$, the presence of FE pairing, i.e., pairing between electrons with different magnetic quantum numbers ($|m_j| = 3/2$ with $|m_j| = 1/2$),

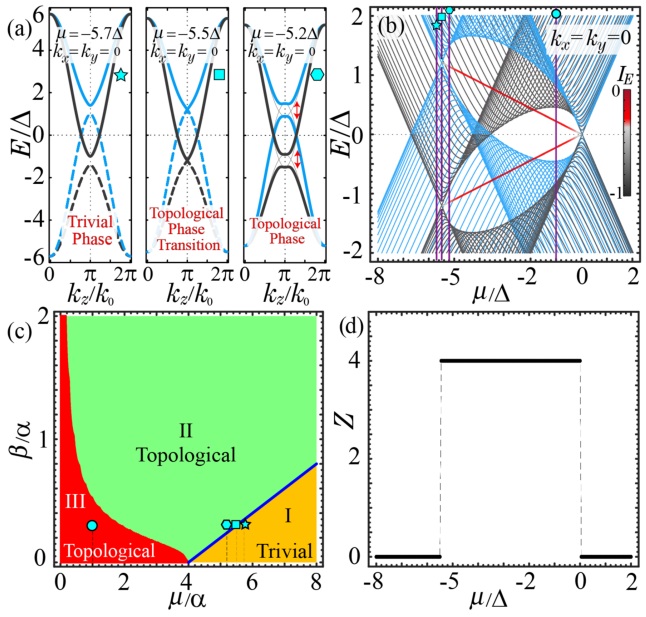

FIG. 1. (a) BdG energy spectra along the [001] direction for three different values of the chemical potential. Solid (dashed) lines depict twofold degenerate particle (hole) bands. Decoupled energy bands are plotted with distinct colors (blue and black) due to $\hat{C}_P$ symmetry. In the third panel, the fade gray lines denote $\Delta = 0$. (b) Spectrum versus μ for a (001) slab with 80 layers. The color bar indicates the inverse participation ratio [82]. The gray and blue colors represent bulk states, and red color denotes edge states. (c) Topological phase diagram induced by FE pairing. Region III (II) indicates that the helical Dirac points are located (coexist with) within the low energy gap (bulk states). (d) Topological invariant corresponding to panel (b). A_{2u} pairing is responsible for superconductivity in all panels. Other parameters are $\beta = 0.3\alpha$, $\alpha = -\Delta$ and $k_0 = a^{-1}$ with a being the lattice constant in corresponding tight-binding calculations.

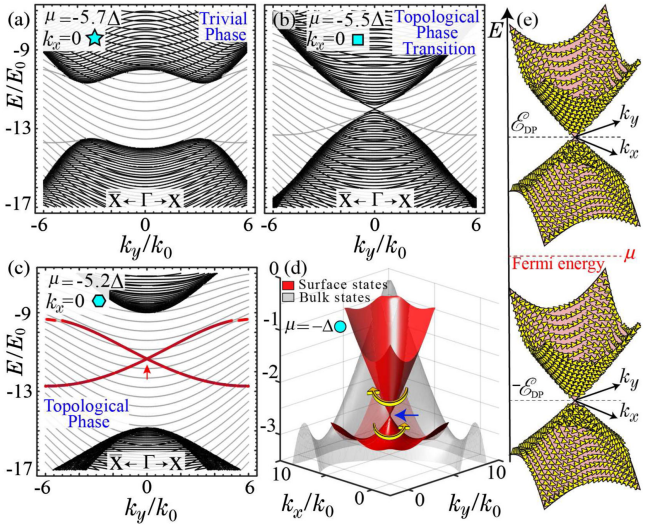

FIG. 2. Spectra of a slab with (001) surfaces as a functions of k_y indicating (a) topologically trivial phase, (b) topological phase transition, and (c) topological phase at FEs. The thickness is 200 layers. (d) 3D energy dispersion versus k_x and k_y. (e) Helical surface cones at positive and negative energies related by particle-hole symmetry. (d),(e) Yellow arrows indicate left- (right-) handed spin texture in the upper (lower) cone. $E_0 = 0.1\Delta$ and other parameters are the same as in Fig. 1.

opens a band gap indicating a TPT. This TPT is accompanied by the emergence of helical topological surface states. To illustrate the appearance of helical surface states (HSSs), the spectrum of a finite system is depicted in Fig. 1(b) [81]. The localized fourfold degenerate HSSs are marked by red indicating large inverse participation ratio (IPR) [82]. They emerge within the range of Fermi energies $\mu/\Delta \in [-5.5, 0]$, in which a nonzero topological invariant, see Fig. 1(d), can be found. We describe below how the topological invariant is defined. Generally, when the energy bands have downward (upward) curvature, i.e., $\mathrm{sgn}(\alpha) = \mathrm{sgn}(\beta) = -(+)1$, the topological phase occurs in the range $\mu/\Delta \in [\mu_c, 0]$ ($[0, \mu_c]$) with the critical value $\mu_c = 4\alpha + 5\beta$. The analysis of the spectrum along other directions reveals that these HSSs are helical topological Dirac points occurring at finite excitation energies as shown in Fig. 2. Notably, the helical surface points do not hybridize with the bulk states due to the combination of time-reversal and twofold rotation symmetries [83].

According to the topological phase diagram, depicted in the plane of $(\mu/\alpha, \beta/\alpha)$ in Fig. 1(c), the FE Cooper pairing in odd-parity multiband superconductors is intrinsically topological (regions II and III) within a certain range of Fermi energies.

Theory for topological phase transition.—The nontrivial topology at FEs originates from unconventional pairing of FE electrons. To understand the underlying mechanism, we project the BdG Hamiltonian onto the doubly degenerate eigenspinors of the normal state $\hat{V}^{\pm}_{\mathbf{k}}$ as the pseudospin basis. In this basis, the interband representation of the BdG Hamiltonian becomes

$$\hat{\mathscr{H}}(\mathbf{k}) = \begin{pmatrix} \hat{\mathsf{H}}^{+-}_{\mathbf{k}} & \hat{\Delta}^{\mathrm{intra}}_{\mathbf{k}} \\ (\hat{\Delta}^{\mathrm{intra}}_{\mathbf{k}})^{\dagger} & \hat{\mathsf{H}}^{-+}_{\mathbf{k}} \end{pmatrix}, \tag{2}$$

where $\hat{\mathsf{H}}^{+-}_{\mathbf{k}}$ and $\hat{\mathsf{H}}^{-+}_{\mathbf{k}}$ denote the interband parts of the BdG Hamiltonian and $\hat{\Delta}^{\mathrm{intra}}_{\mathbf{k}}$ describes intraband pairing at the Fermi energy. The subblock matrices in Eq. (2) can be written as

$$\hat{\mathsf{H}}^{+-}_{\mathbf{k}} = \begin{pmatrix} E^{+}_{\mathbf{k}} & \hat{\Delta}^{+-}_{\mathbf{k}} \\ (\hat{\Delta}^{+-}_{\mathbf{k}})^{\dagger} & -E^{-}_{\mathbf{k}} \end{pmatrix}, \quad \hat{\Delta}^{\mathrm{intra}}_{\mathbf{k}} = \begin{pmatrix} 0 & \hat{\Delta}^{++}_{\mathbf{k}} \\ (\hat{\Delta}^{--}_{\mathbf{k}})^{\dagger} & 0 \end{pmatrix}, \tag{3}$$

where $\hat{\Delta}^{\nu\nu'}_{\mathbf{k}}$ with $\nu, \nu' \in \{+, -\}$ denotes the pairing potential projected onto the normal state bands defined by $\hat{\Delta}^{\nu\nu'}_{\mathbf{k}} = \hat{V}^{\nu\dagger}_{\mathbf{k}} \hat{\Delta}_{\mathbf{k}} (\hat{V}^{\nu'\dagger}_{-\mathbf{k}})^{T}$, where $\nu \neq \nu'$ ($\nu = \nu'$) indicates inter- (intra-) band pairing between electrons having different (identical) magnetic quantum numbers in magnitude. In our model, the most convenient way to explain TPTs at FEs is to make $\hat{\mathscr{H}}(\mathbf{k})$ block diagonal. Thus, TPTs occur in directions in momentum space where the odd-parity interband pairing is finite, whereas the intraband pairing vanishes (nodes at the Fermi energy), i.e., $\hat{\Delta}^{\nu\nu'}_{\mathbf{k}} \neq 0$ and $\hat{\Delta}^{\mathrm{intra}}_{\mathbf{k}} = 0$. These conditions are satisfied, particularly for the A_{2u} pairing, when time-reversal symmetry combines with a twofold rotation around the $\langle 110 \rangle$ direction. This combination is expressed as $\hat{C}_T = \hat{T}\hat{C}_{2,x+y}$ yielding $\hat{C}^2_T = 1$ [62,64,98–104]. Consequently, the point nodes emerge at the Fermi energy accompanied by nonvanishing interband pairing along the $\langle 001 \rangle$ direction. In this case, Eq. (2) becomes block diagonal and $\hat{\mathsf{H}}^{\nu\nu'}_{\mathbf{k}}$ is further reducible. To block diagonalize $\hat{\mathsf{H}}^{\nu\nu'}_{\mathbf{k}}$, we define a general rotation symmetry operator in interband basis

$$\hat{\mathcal{D}}_{\mathbf{n}}(\theta, \epsilon) \equiv \mathrm{diag}(e^{i\theta/2(\mathbf{n}\cdot\hat{\boldsymbol{\tau}})}, \epsilon e^{-i\theta/2(\mathbf{n}\cdot\hat{\boldsymbol{\tau}})^{*}}), \tag{4}$$

where θ is the rotation angle about an arbitrary unit vector $\mathbf{n}$. The vector of Pauli matrices in pseudospin basis is $\hat{\boldsymbol{\tau}} = (\hat{\tau}_x, \hat{\tau}_y, \hat{\tau}_z)$ and $\epsilon = \pm 1$ stands for two unitarily equivalent representations. Along the TPT directions, the superconducting Hamiltonian of each block preserves a two-fold rotation by $\theta = \pi$, i.e., $[\hat{\mathcal{D}}_{\mathbf{n}}(\pi, \epsilon), \hat{\mathsf{H}}^{\nu\nu'}_{\mathbf{k}}] = 0$. This allows us to label the corresponding energy bands by the sign $\pm$ corresponding to the eigenvalues $\lambda = \pm i$ of $\hat{\mathcal{D}}_{\mathbf{n}}(\pi, \epsilon)$. This operation satisfies the property $\hat{\mathcal{D}}^2_{\mathbf{n}}(\pi, \epsilon) = -\hat{\mathbb{1}}$ [105]. $\hat{\mathsf{H}}^{\nu\nu'}_{\mathbf{k}}$ can be reduced to two independent subblock matrices in the eigenspaces of $\hat{\mathcal{D}}_{\mathbf{n}}(\pi, \epsilon)$. The corresponding similarity transformation is $\hat{\mathcal{U}}^{\dagger}\hat{\mathsf{H}}^{\nu\nu'}_{\mathbf{k}}\hat{\mathcal{U}} = \mathrm{diag}(\hat{h}^{\nu\nu'}_{\mathbf{k},-}, \hat{h}^{\nu\nu'}_{\mathbf{k},+})$, where $\hat{\mathcal{U}}$ is the unitary matrix defined by the eigenvectors of $\hat{\mathcal{D}}_{\mathbf{n}}(\pi, \epsilon)$. Then, $\hat{h}^{\nu\nu'}_{\mathbf{k},\lambda}$ becomes

$$\hat{h}^{\nu\nu'}_{\mathbf{k},\lambda} = \begin{pmatrix} -E^{\nu'}_{\mathbf{k}} & (\delta^{\nu\nu'}_{\mathbf{k},\lambda})^* \\ \delta^{\nu\nu'}_{\mathbf{k},\lambda} & E^{\nu}_{\mathbf{k}} \end{pmatrix}, \tag{5}$$

where $\delta^{\nu\nu'}_{\mathbf{k},\lambda}$ is the FE pairing represented in the eigenbasis of $\hat{\mathcal{D}}_{\mathbf{n}}(\pi,\epsilon)$ [106]. Eventually, the transformed BdG Hamiltonian, Eq. (2), decouples into four 2×2 subblocks,

$$\hat{\mathscr{H}}'(\mathbf{k}) = \mathrm{diag}(\hat{h}^{+-}_{\mathbf{k},+}, \hat{h}^{+-}_{\mathbf{k},-}, \hat{h}^{-+}_{\mathbf{k},+}, \hat{h}^{-+}_{\mathbf{k},-}). \tag{6}$$

Note that $\hat{\mathscr{H}}'(\mathbf{k})$ illustrates the decoupling of the double degeneracy of states. For the A_{2u} pairing channel, this is achieved through the mirror reflection symmetry $\hat{C}_P = \hat{P}\hat{C}_{2,x+y}$, where $\hat{P}$ is inversion symmetry, yielding $\hat{C}_P^2 = -1$ [see Fig. 1(a)].

The topological properties at FEs are encoded in the subblocks of $\hat{\mathscr{H}}'(\mathbf{k})$. Generically, when the pairing term in $\hat{h}^{\nu\nu'}_{\mathbf{k},\lambda}$ is odd in momentum, the FE bulk band gaps between electron and hole branches cross or anticross at the parity-invariant momenta. This happens through the tuning of the normal state parameters, i.e., (α,β,μ), and leads to a topologically nontrivial phase as described below.

The topological classification of our 3D model in class DIII is captured by a $\mathbb{Z}$ topological index at low energies [67–71,107]. We are, however, interested in a different type of topological classification at finite excitation energies. This classification is based on the sum of four $\mathbb{Z}_2$ indices stemming form a quantization of the Berry phase defined for each block presented in Eq. (6). Note that $\hat{h}^{+-}_{\mathbf{k},-}$ is essentially a replica of $\hat{h}^{+-}_{\mathbf{k},+}$, owing to the presence of $\hat{\mathcal{D}}_{\mathbf{n}}(\pi,\epsilon)$ symmetry. Additionally, $\hat{h}^{-+}_{\mathbf{k},\pm}$ represent the particle-hole counterparts of $\hat{h}^{+-}_{\mathbf{k},\pm}$. Therefore, the decoupled sectors in Eq. (6) are topologically identical. The topological invariant is given by $Z = \sum_{\lambda\nu\nu'} N^{\nu\nu'}_{\lambda}$ with $\mathbb{Z}_2$ index $N^{\nu\nu'}_{\lambda} = (1/\pi)\oint_c d\mathbf{k}\cdot i\langle u^{\nu\nu'}_{\mathbf{k},\lambda}|\boldsymbol{\nabla}_{\mathbf{k}}|u^{\nu\nu'}_{\mathbf{k},\lambda}\rangle$, where $|u^{\nu\nu'}_{\mathbf{k},\lambda}\rangle$ is the eigenspinor of $\hat{h}^{\nu\nu'}_{\mathbf{k},\lambda}$ associated with the lower energy band [108–111]. In the topological phase, $N^{\nu\nu'}_{\lambda}$ is quantized due to parity symmetry implied by $\hat{\tau}_z\hat{h}^{\nu\nu'}_{\mathbf{k},\lambda}\hat{\tau}_z^{-1} = \hat{h}^{\nu\nu'}_{-\mathbf{k},\lambda}$. We obtain analytically that $\hat{h}^{\nu\nu'}_{\mathbf{k},\lambda}$ is topologically nontrivial with $N^{\nu\nu'}_{\lambda} = 1$, when $\mu/\Delta \in [\mu_c, 0]([0,\mu_c])$ for $\mathrm{sgn}(\alpha) = \mathrm{sgn}(\beta) = -(+)1$. The topological phase diagram in Fig. 1(c) illustrates this analysis [112]. The topological index becomes a net value of $Z = 4$ indicating the emergence of two pairs of helical Dirac states on the surface of superconductor, cf. Fig. 2(e). One helical pair appears at positive excitation energy while the other pair emerges at negative excitation energy [113].

2D surface states.—The HSSs disperse linearly in the vicinity of the Γ point of the 2D surface Brillouin zone as illustrated in Figs. 2(c) and 2(d). At larger momenta, the surface dispersion connects to the bulk states. This is due to the intraband pairing at the Fermi energy, i.e., $\hat{\Delta}^{\mathrm{intra}}_{\mathbf{k}}$. It is finite for nonvanishing k_x or k_y. Hence, $\hat{\mathscr{H}}'(\mathbf{k})$ is no longer block diagonal. This lifts the twofold degeneracy except at the Dirac points, which is the reason for the emergence of helical Dirac surface cones at FEs.

To gain insight into the dispersion of the HSSs, we consider an open surface perpendicular to the z direction and derive an effective Hamiltonian for the HSSs near the Dirac points. We consider k_x and k_y small and decompose the BdG Hamiltonian as $\hat{H}(\mathbf{k}) = \hat{H}(0,0,k_z) + \delta\hat{H}(k_x,k_y,0)$. First, we derive the Dirac point energy at $k_x = k_y = 0$. At this point, $\hat{H}(0,0,k_z)$ becomes block diagonal. This leads to $\hat{\mathscr{H}}'(0,0,k_z) = \mathrm{diag}(\hat{h}^{+-}_{k_z,+}, \hat{h}^{+-}_{k_z,-}, \hat{h}^{-+}_{k_z,+}, \hat{h}^{-+}_{k_z,-})$, which is identical to Eq. (6). We consider a semi-infinite system in the half space $z \geq 0$ with open boundary conditions. Therefore, k_z is no longer conserved and we treat the z direction in real space, where the momentum operator is $-i\partial_z$. The eigenvalue equation for each subblock reads $\hat{h}^{\nu\nu'}_{-i\partial_z,\lambda}\hat{\Phi}(\xi,z) = \mathcal{E}_{\mathrm{DP}}\hat{\Phi}(\xi,z)$, where $\nu,\nu' \in \{+,-\}$ and $\hat{\Phi}(\xi,z) = (u,v)^T\exp(\xi z)$ is the trial eigenspinor of the Dirac point with ξ being its penetration length. $|u|^2$ ($|v|^2$) are probability weights for electron (hole) bands having different band indices. We derive the energy of the helical topological Dirac surface points induced by unconventional FE pairing as

$$\mathcal{E}_{\mathrm{DP}} = \pm\mu\frac{m-m'}{m+m'}, \tag{7}$$

where $m = \alpha + \beta/4$ and $m' = \alpha + 9\beta/4$ are the masses for the normal state bands. Notably, the Dirac points are tunable in energy by chemical potential μ and spin-orbit-coupling strength $m - m' = -2\beta$ [114].

Projecting the BdG Hamiltonian onto the basis of surface states results in an effective Hamiltonian for the FE helical topological surface states of the form [62]

$$\hat{\mathrm{H}}(k_x,k_y) = (\mathcal{E}_{\mathrm{DP}} - \varsigma_1\mathbf{k}_{||}^2)\hat{\sigma}_0 + \varsigma_2(k_y\hat{\sigma}_x - k_x\hat{\sigma}_y), \tag{8}$$

where $\mathbf{k}_{||}^2 = k_x^2 + k_y^2$, and $\varsigma_{1(2)}$ is the group velocity of the HSSs. To leading order, the HSSs exhibit the Dirac dispersion $\mathcal{E}_{\pm} \approx \mathcal{E}_{\mathrm{DP}} \pm \varsigma_2|\mathbf{k}_{||}|$. In the limit, where either μ or $m - m'$ vanishes, the Dirac points shift to zero energy. Then, the FE helical topological surface states become dispersive helical Majorana modes [1–5]. In this case, $\hat{h}^{+-}_{k_z,\pm}$ ($\hat{h}^{-+}_{k_z,\pm}$) resembles an ordinary p-wave superconducting Hamiltonian [115]. However, for finite μ and $m - m'$, topological HSSs emerge at FE.

To identify a proper material to observe this phenomenon, certain conditions need to be satisfied. In the normal state: (i) relevant energy bands should have the same signs of curvature close to the Fermi energy, i.e., both curving downward or upward, (ii) time-reversal symmetry and

twofold rotation should both be present. In the superconducting state: (i) pairing potential should be of odd-parity type, (ii) nodes should be present in the BdG spectrum at the Fermi energy such as in UTe_2 [116], (iii) nonvanishing pairing at FEs should be allowed. Candidates are antiperovskite oxides $Sr_{3-x}SnO$ [117] and half-Heusler materials RPdBi with $R \in \{Y, Dy, Tb, Sm\}$ [72,118]. Specifically, weakly hole-doped YPdBi is a promising material to observe unconventional FE Cooper pairing [72,119]. In the Supplemental Material [62], we combine density functional theory [73–76] and analytical model analysis to estimate the magnitude of FE pairing in holed-doped YPdBi [37,62,77]. We obtain an energy range of $\Delta_E \approx 7.7$–46.2 μeV. Notably, an energy resolution below 8 μeV at operating temperatures of 10 mK is possible via state-of-the-art STM and transport experiments in dilution refrigerators [78]. Hence, FE Cooper pairing should be observable in hole-doped YPdBi.

In addition to the materials mentioned above, hybrid structures such as $BiSbTe_{1.25}Se_{1.75}/NbSe_2$ [56,120], and $Bi_2Te_3/NbSe_2$ [120,121], and X/SBi with $S \in \{YPt, LuPd\}$ [60,66,79], and $X \in \{Si, Ge\}$ are suitable candidates for FE pairing. The excitations in Si, Ge [122], and SBi [60,66] have $j = 3/2$ character near the Fermi energy with suitable curvature. The pairing order parameter in SBi is believed to have p-wave septet symmetry [66,79]. Therefore, the superconducting proximity effect of SBi to Si or Ge should induce FE pairing signaled by the emergence of HSSs.

Conclusions.—We have shown that helical topological superconducting pairing emerges in multiband time-reversal-symmetric odd-parity superconductors due to unconventional pairing away from the Fermi energy. This leads to the appearance of tunable helical topological Dirac surface states at FEs. They are topologically protected against perturbations due to combination of time-reversal and twofold rotation symmetries [62]. Promising experimental probes are (spin-polarized) angle-resolved photoemission [123–131] and scanning tunneling spectroscopies [132–142].

The work was supported by the DFG (SPP 1666, SFB 1170 ToCoTronics, and SFB 1143, project A04, Project-Id 247310070), and the Würzburg-Dresden Cluster of Excellence ct.qmat, EXC 2147, Project-Id 390858490. We thank the Bavarian Ministry of Economic Affairs, Regional Development and Energy for financial support within the High-Tech Agenda Project "Bausteine für das Quanten Computing auf Basis topologischer Materialen." In addition, S. B. Z. acknowledges the support of the start-up fund at HFNL, the Innovation Program for Quantum Science and Technology (Grant No. 2021ZD0302800), and Anhui Initiative in Quantum Information Technologies (Grant No. AHY170000).

*masoud.bahari@uni-wuerzburg.de

[1] B. A. Bernevig, *Topological Insulators and Topological Superconductors* (Princeton University Press, Princeton, NJ, 2013).
[2] M. Z. Hasan, S.-Y. Xu, and G. Bian, Phys. Scr. T **164**, 014001 (2015).
[3] Y. Ando and L. Fu, Annu. Rev. Condens. Matter Phys. **6**, 361 (2015).
[4] M. Sato and Y. Ando, Rep. Prog. Phys. **80**, 076501 (2017).
[5] S. Shen, *Topological Insulators: Dirac Equation in Condensed Matter*, Springer Series in Solid-State Sciences (Springer Singapore, 2017).
[6] L. Fu and C. L. Kane, Phys. Rev. Lett. **100**, 096407 (2008).
[7] X.-L. Qi, T. L. Hughes, S. Raghu, and S.-C. Zhang, Phys. Rev. Lett. **102**, 187001 (2009).
[8] M. Sato, Phys. Rev. B **79**, 214526 (2009).
[9] L. Fu and E. Berg, Phys. Rev. Lett. **105**, 097001 (2010).
[10] Y. S. Hor, A. J. Williams, J. G. Checkelsky, P. Roushan, J. Seo, Q. Xu, H. W. Zandbergen, A. Yazdani, N. P. Ong, and R. J. Cava, Phys. Rev. Lett. **104**, 057001 (2010).
[11] L. A. Wray, S.-Y. Xu, Y. Xia, Y. S. Hor, D. Qian, A. V. Fedorov, H. Lin, A. Bansil, R. J. Cava, and M. Z. Hasan, Nat. Phys. **6**, 855 (2010).
[12] X.-L. Qi and S.-C. Zhang, Rev. Mod. Phys. **83**, 1057 (2011).
[13] C. Fang, B. A. Bernevig, and M. J. Gilbert, Phys. Rev. B **91**, 165421 (2015).
[14] W. Yang, Y. Li, and C. Wu, Phys. Rev. Lett. **117**, 075301 (2016).
[15] Y. Wang, M. Lin, and T. L. Hughes, Phys. Rev. B **98**, 165144 (2018).
[16] E. Khalaf, Phys. Rev. B **97**, 205136 (2018).
[17] D. Călugăru, V. Juričić, and B. Roy, Phys. Rev. B **99**, 041301(R) (2019).
[18] R.-X. Zhang, Y.-T. Hsu, and S. Das Sarma, Phys. Rev. B **102**, 094503 (2020).
[19] R. Joynt and L. Taillefer, Rev. Mod. Phys. **74**, 235 (2002).
[20] M. Sato, Phys. Rev. B **73**, 214502 (2006).
[21] B. Béri, Phys. Rev. B **81**, 134515 (2010).
[22] S. Kobayashi, K. Shiozaki, Y. Tanaka, and M. Sato, Phys. Rev. B **90**, 024516 (2014).
[23] A. P. Schnyder and P. M. R. Brydon, J. Phys. Condens. Matter **27**, 243201 (2015).
[24] D. F. Agterberg, P. M. R. Brydon, and C. Timm, Phys. Rev. Lett. **118**, 127001 (2017).
[25] W. Yang, T. Xiang, and C. Wu, Phys. Rev. B **96**, 144514 (2017).
[26] T. Kawakami, T. Okamura, S. Kobayashi, and M. Sato, Phys. Rev. X **8**, 041026 (2018).
[27] S.-T. Tamura, S. Iimura, and S. Hoshino, Phys. Rev. B **102**, 024505 (2020).
[28] A. K. Nayak, A. Steinbok, Y. Roet, J. Koo, G. Margalit, I. Feldman, A. Almoalem, A. Kanigel, G. A. Fiete, B. Yan, Y. Oreg, N. Avraham, and H. Beidenkopf, Nat. Phys. **17**, 1413 (2021).
[29] A. Moreo, M. Daghofer, A. Nicholson, and E. Dagotto, Phys. Rev. B **80**, 104507 (2009).
[30] L. Komendová, A. V. Balatsky, and A. M. Black-Schaffer, Phys. Rev. B **92**, 094517 (2015).

[31] C. Triola and A. V. Balatsky, Phys. Rev. B **95**, 224518 (2017).
[32] J. Linder and A. V. Balatsky, Rev. Mod. Phys. **91**, 045005 (2019).
[33] G. Tang, C. Bruder, and W. Belzig, Phys. Rev. Lett. **126**, 237001 (2021).
[34] M. Bahari, S.-B. Zhang, and B. Trauzettel, Phys. Rev. Res. **4**, L012017 (2022).
[35] S. Kanasugi and Y. Yanase, Commun. Phys. **5**, 39 (2022).
[36] D. Chakraborty and A. M. Black-Schaffer, Phys. Rev. B **106**, 024511 (2022).
[37] P. Rüßmann, M. Bahari, S. Blügel, and B. Trauzettel, Phys. Rev. Res. **5**, 043181 (2023).
[38] G. Binnig, A. Baratoff, H. E. Hoenig, and J. G. Bednorz, Phys. Rev. Lett. **45**, 1352 (1980).
[39] L. Shan, Y.-L. Wang, B. Shen, B. Zeng, Y. Huang, A. Li, D. Wang, H. Yang, C. Ren, Q.-H. Wang, S. H. Pan, and H.-H. Wen, Nat. Phys. **7**, 325 (2011).
[40] X. Lin, G. Bridoux, A. Gourgout, G. Seyfarth, S. Krämer, M. Nardone, B. Fauqué, and K. Behnia, Phys. Rev. Lett. **112**, 207002 (2014).
[41] S. Kittaka, Y. Aoki, Y. Shimura, T. Sakakibara, S. Seiro, C. Geibel, F. Steglich, H. Ikeda, and K. Machida, Phys. Rev. Lett. **112**, 067002 (2014).
[42] T. Nomoto, K. Hattori, and H. Ikeda, Phys. Rev. B **94**, 174513 (2016).
[43] T. Nomoto and H. Ikeda, Phys. Rev. Lett. **117**, 217002 (2016).
[44] K. Seo, J. D. Sau, and S. Tewari, Phys. Rev. B **95**, 205107 (2017).
[45] Y. Zhao, S. Zeng, C. Lian, Z. Dai, S. Meng, and J. Ni, Phys. Rev. B **98**, 134514 (2018).
[46] J. Singh, A. Jayaraj, D. Srivastava, S. Gayen, A. Thamizhavel, and Y. Singh, Phys. Rev. B **97**, 054506 (2018).
[47] H. Menke, C. Timm, and P. M. R. Brydon, Phys. Rev. B **100**, 224505 (2019).
[48] S. Kanasugi and Y. Yanase, Phys. Rev. B **100**, 094504 (2019).
[49] C. Q. Xu, B. Li, J. J. Feng, W. H. Jiao, Y. K. Li, S. W. Liu, Y. X. Zhou, R. Sankar, N. D. Zhigadlo, H. B. Wang, Z. D. Han, B. Qian, W. Ye, W. Zhou, T. Shiroka, P. K. Biswas, X. Xu, and Z. X. Shi, Phys. Rev. B **100**, 134503 (2019).
[50] J. L. Lado and M. Sigrist, Phys. Rev. Res. **1**, 033107 (2019).
[51] L.-H. Hu, P. D. Johnson, and C. Wu, Phys. Rev. Res. **2**, 022021(R) (2020).
[52] C. Timm and A. Bhattacharya, Phys. Rev. B **104**, 094529 (2021).
[53] T. Shang, W. Xie, J. Z. Zhao, Y. Chen, D. J. Gawryluk, M. Medarde, M. Shi, H. Q. Yuan, E. Pomjakushina, and T. Shiroka, Phys. Rev. B **103**, 184517 (2021).
[54] Z. Wang, S. Zeng, Y. Zhao, X. Wang, and J. Ni, Phys. Rev. B **104**, 174519 (2021).
[55] C. Sevik, J. Bekaert, M. Petrov, and M. V. Milošević, Phys. Rev. Mater. **6**, 024803 (2022).
[56] A. Banerjee, A. Sundaresh, R. Ganesan, and P. S. A. Kumar, ACS Nano **12**, 12665 (2018).
[57] H. Li, T. Zhou, J. He, H.-W. Wang, H. Zhang, H.-C. Liu, Y. Yi, C. Wu, K. T. Law, H. He, and J. Wang, Phys. Rev. B **96**, 075107 (2017).
[58] J. M. Luttinger and W. Kohn, Phys. Rev. **97**, 869 (1955).
[59] G. Dresselhaus, Phys. Rev. **100**, 580 (1955).
[60] P. M. R. Brydon, L. Wang, M. Weinert, and D. F. Agterberg, Phys. Rev. Lett. **116**, 177001 (2016).
[61] The O(3) symmetry-broken case in the normal state is analyzed in the Supplemental Material [62].
[62] See Supplemental Material at http://link.aps.org/supplemental/10.1103/PhysRevLett.132.266201 for additional information about the reasons for TPTs at FE, properties of pseudospin rotation symmetry, global symmetries and an alternative topological index in terms of parity symmetry, O(3) symmetry-broken case and group theoretical analysis, stability of topological surface states under perturbations, derivation of helical Dirac surface states at FEs, the effective surface Hamiltonian, the FE pairing in weakly hole-doped YPdBi, and the pairing matrices in cubic symmetry. The Supplemental Material includes Refs. [13,14,24–27,34,37,52,60,63–78].
[63] L. Savary, J. Ruhman, J. W. F. Venderbos, L. Fu, and P. A. Lee, Phys. Rev. B **96**, 214514 (2017).
[64] J. W. F. Venderbos, L. Savary, J. Ruhman, P. A. Lee, and L. Fu, Phys. Rev. X **8**, 011029 (2018).
[65] J. Yu and C.-X. Liu, Phys. Rev. B **98**, 104514 (2018).
[66] K. Ishihara, T. Takenaka, Y. Miao, Y. Mizukami, K. Hashimoto, M. Yamashita, M. Konczykowski, R. Masuki, M. Hirayama, T. Nomoto, R. Arita, O. Pavlosiuk, P. Wiśniewski, D. Kaczorowski, and T. Shibauchi, Phys. Rev. X **11**, 041048 (2021).
[67] L. Fu and C. L. Kane, Phys. Rev. B **76**, 045302 (2007).
[68] A. P. Schnyder, S. Ryu, A. Furusaki, and A. W. W. Ludwig, Phys. Rev. B **78**, 195125 (2008).
[69] T. L. Hughes, E. Prodan, and B. A. Bernevig, Phys. Rev. B **83**, 245132 (2011).
[70] T. Morimoto and A. Furusaki, Phys. Rev. B **88**, 125129 (2013).
[71] C.-K. Chiu, J. C. Y. Teo, A. P. Schnyder, and S. Ryu, Rev. Mod. Phys. **88**, 035005 (2016).
[72] Y. Nakajima, R. Hu, K. Kirshenbaum, A. Hughes, P. Syers, X. Wang, K. Wang, R. Wang, S. R. Saha, D. Pratt, J. W. Lynn, and J. Paglione, Sci. Adv. **1**, e1500242 (2015).
[73] P. Rüßmann *et al.*, Judftteam/jukkr: v3.6 (2022), 10.5281/zenodo.7284739.
[74] P. Rüßmann and S. Blügel, Phys. Rev. B **105**, 125143 (2022).
[75] A. Jain, S. P. Ong, G. Hautier, W. Chen, W. D. Richards, S. Dacek, S. Cholia, D. Gunter, D. Skinner, G. Ceder, and K. A. Persson, APL Mater. **1**, 011002 (2013).
[76] W. L. Vosko, S. H., and N. M., Can. J. Phys. **58**, 1200 (1980).
[77] V. Bhardwaj, A. Bhattacharya, S. Srivastava, V. V. Khovaylo, J. Sannigrahi, N. Banerjee, B. K. Mani, and R. Chatterjee, Sci. Rep. **11**, 7535 (2021).
[78] J. Schwenk, S. Kim, J. Berwanger, F. Ghahari, D. Walkup, M. R. Slot, S. T. Le, W. G. Cullen, S. R. Blankenship, S. Vranjkovic, H. J. Hug, Y. Kuk, F. J. Giessibl, and J. A. Stroscio, Rev. Sci. Instrum. **91**, 071101 (2020).

[79] H. Kim, K. Wang, Y. Nakajima, R. Hu, S. Ziemak, P. Syers, L. Wang, H. Hodovanets, J. D. Denlinger, P. M. R. Brydon, D. F. Agterberg, M. A. Tanatar, R. Prozorov, and J. Paglione, Sci. Adv. **4**, eaao4513 (2018).

[80] Our table is slightly different from the results given in Ref. [63]. The details of our calculations are given explicitly in the Supplemental Material [62].

[81] To evaluate the tight-binding calculations, we used standard lattice regularizations $k_z^2 \to 2[1-\cos(k_z a)]/a^2$ and $k_z \to \sin(k_z a)/a$, where a is the lattice constant.

[82] The IPR is defined by $I_E = \ln[\sum_{i=1}^{8N} |\langle i|\psi\rangle|^4 / \ln(8N)]$ where N is the total number of sites and $|\psi\rangle$ indicates the eigenvector associated to E. The localized (extended) boundary (bulk) states have $I_E \to 0(-1)$.

[83] Such a coexistence establishes topological bound states in the continuum (BIC). This has been addressed in different quantum mechanical systems [84–97]. However, the emergent topological BIC intrinsically induced by FE superconducting correlations has not been reported so far.

[84] Y. Plotnik, O. Peleg, F. Dreisow, M. Heinrich, S. Nolte, A. Szameit, and M. Segev, Phys. Rev. Lett. **107**, 183901 (2011).

[85] J. Mur-Petit and R. A. Molina, Phys. Rev. B **90**, 035434 (2014).

[86] Y. Baum, T. Posske, I. C. Fulga, B. Trauzettel, and A. Stern, Phys. Rev. Lett. **114**, 136801 (2015).

[87] C. W. Hsu, B. Zhen, A. D. Stone, J. D. Joannopoulos, and M. Soljavcic, Nat. Rev. Mater. **1**, 16048 (2016).

[88] L. S. Ricco, Y. Marques, F. A. Dessotti, R. S. Machado, M. de Souza, and A. C. Seridonio, Phys. Rev. B **93**, 165116 (2016).

[89] Y.-X. Xiao, G. Ma, Z.-Q. Zhang, and C. T. Chan, Phys. Rev. Lett. **118**, 166803 (2017).

[90] S. Mukherjee, J. Gomis-Bresco, P. Pujol-Closa, D. Artigas, and L. Torner, Phys. Rev. A **98**, 063826 (2018).

[91] M. Bahari and M. V. Hosseini, Phys. Rev. B **99**, 155128 (2019).

[92] M. Takeichi and S. Murakami, Phys. Rev. B **99**, 035128 (2019).

[93] Z.-G. Chen, C. Xu, R. Al Jahdali, J. Mei, and Y. Wu, Phys. Rev. B **100**, 075120 (2019).

[94] M. Jangjan and M. V. Hosseini, Sci. Rep. **10**, 14256 (2020).

[95] W. A. Benalcazar and A. Cerjan, Phys. Rev. B **101**, 161116(R) (2020).

[96] A. Cerjan, M. Jürgensen, W. A. Benalcazar, S. Mukherjee, and M. C. Rechtsman, Phys. Rev. Lett. **125**, 213901 (2020).

[97] Z. Gong, J. Serafini, F. Yang, S. Preble, and J. Yao, Phys. Rev. Appl. **16**, 024059 (2021).

[98] The combination of time-reversal symmetry and twofold crystalline rotation symmetry has been explored in prior works [99–104]. However, to the best of our knowledge, the prediction of finite energy pairing gaps with nontrivial topology is exclusive to our Letter.

[99] C. Fang and L. Fu, Phys. Rev. B **91**, 161105(R) (2015).

[100] F. Schindler, Z. Wang, M. G. Vergniory, A. M. Cook, A. Murani, S. Sengupta, A. Y. Kasumov, R. Deblock, S. Jeon, I. Drozdov, H. Bouchiat, S. Guéron, A. Yazdani, B. A. Bernevig, and T. Neupert, Nat. Phys. **14**, 918 (2018).

[101] C. Fang and L. Fu, Sci. Adv. **5**, eaat2374 (2019).

[102] H. Li and K. Sun, Phys. Rev. B **102**, 085108 (2020).

[103] H. Li and S. Wan, Phys. Rev. B **104**, 045150 (2021).

[104] J. Henke, M. Kurttutan, J. Kruthoff, and J. van Wezel, Phys. Rev. B **104**, L201110 (2021).

[105] The basis elements of $\hat{\mathsf{H}}_{\mathbf{k}}^{+-}$ under two-fold rotation about the x (y) axis flips the orientation of the pseudospin indices $\{\uparrow,\downarrow\} \leftrightarrow \{\downarrow,\uparrow\}$, while the momentum remains intact. In our model, the pseudospin up (down) is composed of a linear combination of magnetic quantum numbers $m_j \in \{\pm 1/2, \pm 3/2\}$.

[106] Note that $\hat{h}_{\mathbf{k},\lambda}^{-+}$ can be easily derived by substitution of $+ \leftrightarrow -$ in Eq. (5). $\delta_{\mathbf{k},\lambda}^{+-}$ fulfills the symmetry relation $\delta_{\mathbf{k},\lambda}^{-+} = -\delta_{-\mathbf{k},\lambda}^{+-}$.

[107] The BdG Hamiltonian preserves time-reversal $\hat{T}$, particle-hole $\hat{\mathscr{P}}$, chiral $\hat{\mathcal{C}}$, and inversion $\hat{\mathcal{P}}_u$ symmetries. The symmetry operators fulfill the properties $\hat{T}^2 = -1$ and $\hat{\mathscr{P}}^2 = \hat{\mathcal{P}}_u^2 = 1$.

[108] M. V. Berry, Proc. R. Soc. A **392**, 45 (1984).

[109] J. Zak, Phys. Rev. Lett. **62**, 2747 (1989).

[110] R. Resta, Rev. Mod. Phys. **66**, 899 (1994).

[111] D. Xiao, M.-C. Chang, and Q. Niu, Rev. Mod. Phys. **82**, 1959 (2010).

[112] The FE topological Dirac surface states are not restricted to the A_{2u} channel. Rather, they also exist for the other pairing channels summarized in Table I. The TPTs at FEs happen along the C_2 axes for the E_u and T_{2u} channels, and along the C_2' axes for the T_{2u} channel.

[113] The Dirac points are twofold degenerate at one surface at positive and at negative excitation energies. Considering two surfaces, we obtain the same set of Dirac points on each surface. Thus, the degeneracy is doubled as compared to the case of single surface.

[114] Although, spin-orbit coupling is an essential ingredient for the formation of such surface states in our model, the effective masses in systems with nearly vanishing spin-orbit coupling can stem from different orbitals giving rise to nonvanishing values for $m - m'$.

[115] A. Y. Kitaev, Phys. Usp. **44**, 131 (2001).

[116] T. Metz, S. Bae, S. Ran, I. L. Liu, Y. S. Eo, W. T. Fuhrman, D. F. Agterberg, S. M. Anlage, N. P. Butch, and J. Paglione, Phys. Rev. B **100**, 220504(R) (2019).

[117] M. Oudah, A. Ikeda, J. N. Hausmann, S. Yonezawa, T. Fukumoto, S. Kobayashi, M. Sato, and Y. Maeno, Nat. Commun. **7**, 13617 (2016).

[118] The inversion breaking antisymmetric spin-orbit-coupling (ASOC) in half-Heusler material is weak compared to symmetric spin-orbit coupling.

[119] S. M. A. Radmanesh, C. Martin, Y. Zhu, X. Yin, H. Xiao, Z. Q. Mao, and L. Spinu, Phys. Rev. B **98**, 241111(R) (2018).

[120] X. Xi, Z. Wang, W. Zhao, J.-H. Park, K. T. Law, H. Berger, L. Forró, J. Shan, and K. F. Mak, Nat. Phys. **12**, 139 (2016).

[121] H. Zhang, C.-X. Liu, X.-L. Qi, X. Dai, Z. Fang, and S.-C. Zhang, Nat. Phys. **5**, 438 (2009).

[122] M. Grundmann, *The Physics of Semiconductors: An Introduction Including Devices and Nanophysics* (Springer, Berlin Heidelberg, 2006).
[123] D. Hsieh, Y. Xia, L. Wray, D. Qian, A. Pal, J. H. Dil, J. Osterwalder, F. Meier, G. Bihlmayer, C. L. Kane, Y. S. Hor, R. J. Cava, and M. Z. Hasan, Science **323**, 919 (2009).
[124] Y. Zhang, L. X. Yang, M. Xu, Z. R. Ye, F. Chen, C. He, H. C. Xu, J. Jiang, B. P. Xie, J. J. Ying, X. F. Wang, X. H. Chen, J. P. Hu, M. Matsunami, S. Kimura, and D. L. Feng, Nat. Mater. **10**, 273 (2011).
[125] D. V. Evtushinsky, V. B. Zabolotnyy, T. K. Kim, A. A. Kordyuk, A. N. Yaresko, J. Maletz, S. Aswartham, S. Wurmehl, A. V. Boris, D. L. Sun, C. T. Lin, B. Shen, H. H. Wen, A. Varykhalov, R. Follath, B. Büchner, and S. V. Borisenko, Phys. Rev. B **89**, 064514 (2014).
[126] E. J. Sie, T. Rohwer, C. Lee, and N. Gedik, Nat. Commun. **10**, 3535 (2019).
[127] J. J. P. Thompson, D. Pei, H. Peng, H. Wang, N. Channa, H. L. Peng, A. Barinov, N. B. M. Schröter, Y. Chen, and M. Mucha-Kruczyński, Nat. Commun. **11**, 3582 (2020).
[128] W. Liu, L. Cao, S. Zhu, L. Kong, G. Wang, M. Papaj, P. Zhang, Y.-B. Liu, H. Chen, G. Li, F. Yang, T. Kondo, S. Du, G.-H. Cao, S. Shin, L. Fu, Z. Yin, H.-J. Gao, and H. Ding, Nat. Commun. **11**, 5688 (2020).
[129] C. Liu, R. P. Day, F. Li, R. L. Roemer, S. Zhdanovich, S. Gorovikov, T. M. Pedersen, J. Jiang, S. Lee, M. Schneider, D. Wong, P. Dosanjh, F. J. Walker, C. H. Ahn, G. Levy, A. Damascelli, G. A. Sawatzky, and K. Zou, Nat. Commun. **12**, 4573 (2021).
[130] C. Lin, M. Ochi, R. Noguchi, K. Kuroda, M. Sakoda, A. Nomura, M. Tsubota, P. Zhang, C. Bareille, K. Kurokawa, Y. Arai, K. Kawaguchi, H. Tanaka, K. Yaji, A. Harasawa, M. Hashimoto, D. Lu, S. Shin, R. Arita, S. Tanda, and T. Kondo, Nat. Mater. **20**, 1093 (2021).
[131] S.-D. Chen, M. Hashimoto, Y. He, D. Song, J.-F. He, Y.-F. Li, S. Ishida, H. Eisaki, J. Zaanen, T. P. Devereaux, D.-H. Lee, D.-H. Lu, and Z.-X. Shen, Nature (London) **601**, 562 (2022).
[132] M. Bode, Rep. Prog. Phys. **66**, 523 (2003).
[133] J. Wiebe, A. Wachowiak, F. Meier, D. Haude, T. Foster, M. Morgenstern, and R. Wiesendanger, Rev. Sci. Instrum. **75**, 4871 (2004).
[134] Z. Alpichshev, J. G. Analytis, J.-H. Chu, I. R. Fisher, Y. L. Chen, Z. X. Shen, A. Fang, and A. Kapitulnik, Phys. Rev. Lett. **104**, 016401 (2010).
[135] O. Fischer, M. Kugler, I. Maggio-Aprile, C. Berthod, and C. Renner, Rev. Mod. Phys. **79**, 353 (2007).
[136] H. Oka, O. O. Brovko, M. Corbetta, V. S. Stepanyuk, D. Sander, and J. Kirschner, Rev. Mod. Phys. **86**, 1127 (2014).
[137] M. Neupane, N. Alidoust, M. M. Hosen, J.-X. Zhu, K. Dimitri, S.-Y. Xu, N. Dhakal, R. Sankar, I. Belopolski, D. S. Sanchez, T.-R. Chang, H.-T. Jeng, K. Miyamoto, T. Okuda, H. Lin, A. Bansil, D. Kaczorowski, F. Chou, M. Z. Hasan, and T. Durakiewicz, Nat. Commun. **7**, 13315 (2016).
[138] L. Cornils, A. Kamlapure, L. Zhou, S. Pradhan, A. A. Khajetoorians, J. Fransson, J. Wiebe, and R. Wiesendanger, Phys. Rev. Lett. **119**, 197002 (2017).
[139] D.-J. Choi, C. Rubio-Verdú, J. de Bruijckere, M. M. Ugeda, N. Lorente, and J. I. Pascual, Nat. Commun. **8**, 15175 (2017).
[140] P. Fan, F. Yang, G. Qian, H. Chen, Y.-Y. Zhang, G. Li, Z. Huang, Y. Xing, L. Kong, W. Liu, K. Jiang, C. Shen, S. Du, J. Schneeloch, R. Zhong, G. Gu, Z. Wang, H. Ding, and H.-J. Gao, Nat. Commun. **12**, 1348 (2021).
[141] D. Wang, J. Wiebe, R. Zhong, G. Gu, and R. Wiesendanger, Phys. Rev. Lett. **126**, 076802 (2021).
[142] L. Schneider, P. Beck, J. Wiebe, and R. Wiesendanger, Sci. Adv. **7**, eabd7302 (2021).